USER GUIDE
Planetary-Code-Collection:
Thermal and Ice Evolution Models
for Planetary Surfaces

Norbert Schörghofer (norbert@hawaii.edu)

2002–2017
Last updated July 17, 2017

Contents

Preface

Companion to https://github.com/nschorgh/Planetary-Code-Collection/

Technical Notes:
Most of the code was developed with a `gfortran` compiler on MacOS X with an Intel processor. Many components were also run on various Linux clusters, sometimes using other compilers. The non-portable `real(8)` is meant to correspond to an 8-byte floating point number.

Part 1

Conduction of Heat

1-Dimensional Numerical Model of Thermal Conduction in the Planetary Subsurface

Authors & History: originally implemented by Samar Khatiwala in 2001 (including upper radiation boundary condition for semi-implicit scheme); extended to variable thermal properties and irregular grid by Norbert Schörghofer 2002–2003

1.1 Governing Equation

T ... temperature, t ... time, z ... depth, ρc ... volumetric heat capacity, k ... thermal conductivity

$$\rho c \frac{\partial T}{\partial t} = \frac{\partial}{\partial z}\left(k\frac{\partial T}{\partial z}\right) \tag{1.1}$$

$F = k\dfrac{\partial T}{\partial z}$ ... heat flux
various boundary conditions

1.2 Semi-Implicit Scheme on Irregular Grid

$$\frac{\partial}{\partial z}F_j = \frac{F_{j+\frac{1}{2}} - F_{j-\frac{1}{2}}}{(z_{j+1}-z_{j-1})/2} = 2\frac{k_{j+\frac{1}{2}}\frac{T_{j+1}-T_j}{z_{j+1}-z_j} - k_{j-\frac{1}{2}}\frac{T_j-T_{j-1}}{z_j-z_{j-1}}}{z_{j+1}-z_{j-1}}$$

$$(\rho c)_j\frac{\partial T_j}{\partial t} = \frac{2k_{j+\frac{1}{2}}}{(z_{j+1}-z_j)(z_{j+1}-z_{j-1})}T_{j+1} - \frac{2}{z_{j+1}-z_{j-1}}\left(\frac{k_{j+\frac{1}{2}}}{z_{j+1}-z_j} + \frac{k_{j-\frac{1}{2}}}{z_j-z_{j-1}}\right)T_j +$$

$$+\frac{2k_{j-\frac{1}{2}}}{(z_j-z_{j-1})(z_{j+1}-z_{j-1})}T_{j-1}$$

$$\text{introduce}\quad \alpha_j = \frac{\Delta t}{(\rho c)_j}\frac{k_{j+\frac{1}{2}}}{(z_{j+1}-z_j)(z_{j+1}-z_{j-1})} \quad\text{and}\quad \gamma_j = \frac{\Delta t}{(\rho c)_j}\frac{k_{j-\frac{1}{2}}}{(z_j-z_{j-1})(z_{j+1}-z_{j-1})} \tag{1.2}$$

$$\Delta t\frac{\partial T_j}{\partial t} = 2\alpha_j T_{j+1} - 2(\alpha_j + \gamma_j)T_j + 2\gamma_j T_{j-1}$$

$$T_j^{n+1} - T_j^n = \alpha_j T_{j+1}^{n+1} - (\alpha_j + \gamma_j)T_j^{n+1} + \gamma_j T_{j-1}^{n+1} + \alpha_j T_{j+1}^n - (\alpha_j + \gamma_j)T_j^n + \gamma_j T_{j-1}^n$$

$$\boxed{-\alpha_j T_{j+1}^{n+1} + (1 + \alpha_j + \gamma_j)T_j^{n+1} - \gamma_j T_{j-1}^{n+1} = \alpha_j T_{j+1}^n + (1 - \alpha_j - \gamma_j)T_j^n + \gamma_j T_{j-1}^n}\quad 1 < j < N \tag{1.3}$$

Superscript n refers to time step. Subscript j refers to position z_j. The conductivity k is defined on half-points. In the program, $2(\rho c)_j = (\rho c)_{j+\frac{1}{2}} + (\rho c)_{j-\frac{1}{2}}$. In this way, the parameters k and ρc do not need to be defined at an interface of two layers with different thermal properties. Since indices in the program must be integers, we choose $k(j) = k_{j-\frac{1}{2}}$ and the same for ρc.

1.2.1 Upper boundary condition:

a) Radiation

$$Q + k\left.\frac{\partial T}{\partial z}\right|_{z=0} = \left.\epsilon\sigma T^4\right|_{z=0} \tag{1.4}$$

Q is the incoming solar flux including the atmospheric contribution.
introduce auxiliary quantity T_0, such that surface temperature $T_s = (T_0 + T_1)/2$

$$\left.\frac{\partial T}{\partial z}\right|_{z=0} = \frac{T_1 - T_0}{\Delta z} \quad \text{and} \quad \left.T^4\right|_{z=0} = \left(\frac{T_0 + T_1}{2}\right)^4 \quad \text{with} \quad \Delta z = 2z_1$$

$T = T_r + T'$ $\qquad T_r$ is a reference temperature around which we linearize

$$
\begin{aligned}
Q + k_{1/2}\frac{T_1 - T_0}{\Delta z} &= \epsilon\sigma\left(\frac{2T_r + T_0' + T_1'}{2}\right)^4 \\
&\approx \epsilon\sigma T_r^4 + 2\epsilon\sigma T_r^3(T_0' + T_1') \\
&= -3\epsilon\sigma T_r^4 + 2\epsilon\sigma T_r^3(T_0 + T_1)
\end{aligned}
$$

$T_0\left(\frac{k_{1/2}}{\Delta z} + B(T_r)\right) = Q + 3\epsilon\sigma T_r^4 + T_1\left(\frac{k_{1/2}}{\Delta z} - B(T_r)\right)$ where $B(T_r) = 2\epsilon\sigma T_r^3$
introduce $a = (Q + 3\epsilon\sigma T_r^4)/(\frac{k}{\Delta z} + B)$ and $b = (\frac{k_{1/2}}{\Delta z} - B)/(\frac{k_{1/2}}{\Delta z} + B)$

$$-\alpha_1 T_2^{n+1} + (1 + \alpha_1 + \gamma_1 - \gamma_1 b^n)T_1^{n+1} = \alpha_1 T_2^n + (1 - \alpha_1 - \gamma_1 + \gamma_1 b^n)T_1^n + \gamma_1\frac{Q^n + Q^{n+1} + 6\epsilon\sigma T_r^4}{\frac{k_{1/2}}{\Delta z} + B^n}$$

choose $\Delta z = z_2 - z_1 = 2z_1$, define $\beta = \frac{\Delta t}{(\rho c)_1}\frac{1}{2\Delta z^2}$, then $\alpha_1 = \beta k_{3/2}$ and $\gamma_1 = \beta k_{1/2}$

$$\text{surface temperature} \quad T_s = \frac{1}{2}(T_1 + T_0) = \frac{1}{2}\left(\frac{Q + 3\epsilon\sigma T_r^4}{k_{1/2}/\Delta z + B} + T_1 + bT_1\right) = \frac{Q + 3\epsilon\sigma T_r^4 + \frac{2k}{\Delta z}T_1}{2(k_{1/2}/\Delta z + B)}$$

choose $T_r^n = T_s^{n-1}$
implemented in `conductionQ.f`

b) prescribed T

standard formulas (1.2,1.3) with $T_0 = T_s$ and $z_0 = 0$

$$\alpha_1 = \frac{\Delta t}{(\rho c)_1}\frac{k_{3/2}}{(z_2 - z_1)z_2}, \qquad \gamma_1 = \frac{\Delta t}{(\rho c)_1}\frac{k_{1/2}}{z_1 z_2}$$

$$-\alpha_1 T_2^{n+1} + (1 + \alpha_1 + \gamma_1)T_1^{n+1} = \alpha_1 T_2^n + (1 - \alpha_1 - \gamma_1)T_1^n + \gamma_1(T_s^n + T_s^{n+1})$$

implemented in `conductionT.f`

4

1.2.2   Lower boundary condition:

(assume $z_{N+1} - z_N = z_N - z_{N-1}$)

No heat flux: $F_{N+\frac{1}{2}} = 0 \quad \Rightarrow \quad k_{N+\frac{1}{2}}(T_{N+1} - T_N) = 0 \quad \Rightarrow \quad T_{N+1} = T_N$

$$(1 + \gamma_N)T_N^{n+1} - \gamma_N T_{N-1}^{n+1} = (1 - \gamma_N)T_N^n + \gamma_N T_{N-1}^n$$

$$\gamma_N = \frac{\Delta t}{(\rho c)_N} \frac{k_{N-\frac{1}{2}}}{2(z_N - z_{N-1})^2}$$

Or geothermal heating: $F_{N+\frac{1}{2}} = F_{\text{geothermal}} \quad \Rightarrow \quad k_{N+\frac{1}{2}}(T_{N+1} - T_N) = \Delta z F_{\text{geothermal}}$

$$(1 + \gamma_N)T_N^{n+1} - \gamma_N T_{N-1}^{n+1} = (1 - \gamma_N)T_N^n + \gamma_N T_{N-1}^n + \frac{\Delta t}{(\rho c)_N} \frac{F_{\text{geothermal}}}{\Delta z}$$

1.3   With Frost Cover (Mars)

Add latent heat of CO_2 sublimation

$$Q + k \left.\frac{\partial T}{\partial z}\right|_{z=0} = \epsilon \sigma T^4 \big|_{z=0} + L \frac{dm_{CO_2}}{dt} \tag{1.5}$$

call `conductionQ` if T_s is above CO_2 frost point or if $m_{CO_2} = 0$; call `conductionT` if T_s is below CO_2 frost point or if $m_{CO_2} > 0$; calculate energy difference and add CO_2 mass; adjust surface albedo; repeat this at every time step

1.4   Influence of Ice on Thermal Properties

This is only one possible parametrization. In retrospective, it agrees well with the laboratory measurements by Siegler et al. (2012).

$$\begin{aligned}
\rho c &= (1 - \epsilon)\rho_{\text{regolith}} c_{\text{regolith}} + \epsilon f \rho_{\text{ice}} c_{\text{ice}} \\
k &= (1 - \epsilon)k_{\text{regolith}} + \epsilon f k_{\text{ice}} + (1 - f)\epsilon k_{\text{air}}
\end{aligned}$$

ρ ... density; c ... heat capacity; k ... thermal conductivity
ϵ ... porosity (void space / total volume)
f ... ice filling fraction ($f = \rho_f / \rho_{\text{ice}}$, ρ_f =density of free ice)
Observed from orbit is ice-three thermal inertia I.

at around 200 Kelvin: $c_{\text{ice}} \approx 1540$ J/(kg K), $\rho_{\text{ice}} \approx 927$ kg/m^3, $k_{\text{ice}} \approx 3.2$ W/(m K)
See Winter and Saari (1969) for heat capacity of silicates as a function of temperature.
See Handbook of Chemistry and Physics (Lide, 2003) for temperature dependence for ice.

In the program, k and ρc are defined on half-points, while ρ_f and T are defined on grid points.

Used in Schorghofer and Aharonson (2005) and as part of many subsequent modeling papers.

Bibliography

D. R. Lide, editor. *CRC Handbook of Chemistry and Physics*. CRC Press, 84th edition, 2003.

N. Schorghofer and O. Aharonson. Stability and exchange of subsurface ice on Mars. *J. Geophys. Res.*, 110(E5):E05003, 2005.

M. Siegler, O. Aharonson, E. Carey, M. Choukroun, T.L. Hudson, N. Schorghofer, and S. Xu. Measurements of thermal properties of icy Mars regolith analogs. *J. Geophys. Res.*, 117:E03001, 2012.

D. F. Winter and J. M. Saari. A particulate thermophysical model of the lunar soil. *Astrophys. J.*, 156:1135–1151, 1969.

Part 2

Diffusion of Water Vapor with Phase Transitions

1-Dimensional Diffusion of Water Vapor in Porous Medium with Phase Transitions;
variable diffusivity; irregular grid
3 phases: vapor, free (macroscopic) H_2O ice, H_2O adsorbate
implemented in `vapordiffusioni.f`

History: developed 2003–2004

2.1 Governing Equations

indices: v ... gas (vapor), f ... free ice (solid), a ... adsorbed water
$\bar{\rho}$ ... mass per total volume, $\bar{J}$ ... vapor flux per total area

conservation of mass:
$$\frac{\partial}{\partial t}(\bar{\rho}_v + \bar{\rho}_f + \bar{\rho}_a) + \nabla \cdot \bar{J} = 0 \tag{2.1}$$

vapor transport: (Landau and Lifshitz, 1987, Vol. VI, §57, §58)

$$J = -D\rho_0 \nabla c \tag{2.2}$$

c ... concentration $c = \rho_v/\rho_0$
ρ_{air} ... total density of air, including humidity
ρ_v ... density of vapor

$$p_v = nkT = \rho_v \frac{k}{m_v} T \tag{2.3}$$

m ... mass of molecule; k ... Boltzmann constant

adsorption: $\bar{\rho}_a = A(p, T)$
The amount adsorbed also changes when ice is present.

ϵ ... porosity (= void space / total volume)
$\epsilon(1 - \rho_f/\rho_{\text{ice}})$ ... fraction of space available to gas
$\bar{\rho}_v = \rho_v \epsilon (1 - \rho_f/\rho_{\text{ice}})$ $\qquad$ ρ_v ... vapor density in void space
$\bar{\rho}_f = \rho_f \epsilon$ $\qquad\qquad\qquad$ ρ_f ... ice density in volume not occupied by regolith
$\bar{J} = J\epsilon(1 - \rho_f/\rho_{\text{ice}})$ $\qquad$ J ... vapor flux through void area

$\rho_{\text{ice}} \approx 926 \text{ kg/m}^3$ ... density of ice when it's really cold

Conservation of mass becomes

$$\frac{\partial}{\partial t}\left(\rho_v\left(1 - \frac{\rho_f}{\rho_{\text{ice}}}\right) + \rho_f + \frac{1}{\epsilon}\bar{\rho}_a\right) + \partial_z\left(1 - \frac{\rho_f}{\rho_{\text{ice}}}\right)J = 0$$

$$\frac{\partial}{\partial t}\left[\rho_v\left(1 - \frac{\rho_f}{\rho_{\text{ice}}}\right) + \rho_f + \frac{1}{\epsilon}\bar{\rho}_a\right] = \partial_z\left[\left(1 - \frac{\rho_f}{\rho_{\text{ice}}}\right)D\partial_z\rho_v\right]$$

introduce $\varphi = 1 - \dfrac{\rho_f}{\rho_{\text{ice}}}$ and $\gamma = \dfrac{k}{m}\dfrac{1}{\epsilon}$

$$\partial_t\left(\frac{p}{T}\varphi + \frac{k}{m_v}\rho_f\right) + \gamma\left(\frac{\partial\bar{\rho}_a}{\partial p}\partial_t p + \frac{\partial\bar{\rho}_a}{\partial T}\partial_t T\right) = \partial_z\left[D\varphi\left(\partial_z\frac{p}{T}\right)\right] \tag{2.4}$$

This is an equation for p and ρ_f.

If there is no ice, then

$$\left(\frac{1}{T} + \gamma\frac{\partial\bar{\rho}_a}{\partial p}\right)\partial_t p + \left(-\frac{p}{T^2} + \gamma\frac{\partial\bar{\rho}_a}{\partial T}\right)\partial_t T = \partial_z\left(D\partial_z\frac{p}{T}\right)$$

2.2   Discretizations

2.2.1   Possible discretizations of spatial derivatives:

Note: These spatial discretizations are not necessarily optimal in terms of discretization error.

$$\partial_z(a\partial_z b)|_j = \frac{1}{\Delta z^2}\left(a_{j+1/2}(b_{j+1} - b_j) - a_{j-1/2}(b_j - b_{j-1})\right) + O(\Delta z^2) \tag{2.5}$$

or

$$\partial_z(a\partial_z b)|_j = \frac{1}{2\Delta z^2}\left((a_{j+1} + a_j)(b_{j+1} - b_j) - (a_j + a_{j-1})(b_j - b_{j-1})\right) + O(\Delta z^2) \tag{2.6}$$

or

$$\begin{aligned}
\partial_z(a\partial_z b)|_j &= a\partial_{zz}b + (\partial_z a)\partial_z b \\
&= \frac{1}{\Delta z^2}\left(a_j(b_{j+1} - 2b_j + b_{j-1}) + \frac{1}{4}(a_{j+1} - a_{j-1})(b_{j+1} - b_{j-1})\right) + O(\Delta z^2) \quad (2.7)
\end{aligned}$$

The most general discretization which is accurate to $O(\Delta z^2)$, rather than just $O(\Delta z)$, is of the following form (mathematica notebook discretization2.nb)

$$\begin{aligned}
\partial_z(a\partial_z b)|_j &= \frac{1}{\Delta z^2}(ca_j b_j + (-1 - \frac{c}{2})a_{j-1}b_j + (-1 - \frac{c}{2})a_{j+1}b_j \\
&\quad -\frac{c}{2}a_j b_{j-1} + \frac{3+c}{4}a_{j-1}b_{j-1} + \frac{1+c}{4}a_{j+1}b_{j-1} \\
&\quad -\frac{c}{2}a_j b_{j+1} + \frac{1+c}{4}a_{j-1}b_{j+1} + \frac{3+c}{4}a_{j+1}b_{j+1}) + O(\Delta z^2) \tag{2.8}
\end{aligned}$$

Choices (2.6) and (2.7) above correspond to $c = -1$ and $c = -2$, respectively.

Another set of schemes are the ones that do not involve the corner points $a_{j+1}b_{j-1}$ and $a_{j-1}b_{j+1}$. They are of the following form (mathematica notebook discretization3.nb)

$$
\begin{aligned}
\partial_z(a\partial_z b)|_j &= \frac{1}{\Delta z^2}(-a_j b_j - c a_{j-1} b_j + (-1+c)a_{j+1}b_j + \\
&\quad (1-c)a_j b_{j-1} + c a_{j-1} b_{j-1} + c a_j b_{j+1} + (1-c)a_{j+1}b_{j+1}) + \\
&\quad \left(c - \frac{1}{2}\right)O(\Delta z) + O(\Delta z^2) \\
&= \frac{1}{\Delta z^2}[(1-c)a_{j+1}(b_{j+1} - b_j) + c a_{j-1}(b_{j-1} - b_j) + a_j(c b_{j+1} - b_j + (1-c)b_{j-1})] + O(\Delta z)
\end{aligned}
\tag{2.9}
$$

For $c = 1/2$ this reduces to scheme (2.6) above
If starting with complete pore filling, $c > 0$ is required for downward motion of ice table.

On irregular grid: General scheme without corner points (mathematica notebook discretization6.nb)

$$
\begin{aligned}
\partial_z(a\partial_z b)|_j &= -\frac{2c + (1-2c)h_+/h_-}{h_- h_+}a_j b_j + \frac{-1 + (1-2c)h_+/h_-}{h_-(h_- + h_+)}a_{j-1}b_j + \frac{2c-2}{h_+(h_- + h_+)}a_{j+1}b_j + \\
&\quad +\frac{1 + (1-2c)h_+/h_-}{h_-(h_- + h_+)}a_j b_{j-1} + \frac{1 + (2c-1)h_+/h_-}{h_-(h_- + h_+)}a_{j-1}b_{j-1} + \frac{2c}{h_+(h_- + h_+)}a_j b_{j+1} \\
&\quad +\frac{2-2c}{h_+(h_- + h_+)}a_{j+1}b_{j+1} + O(h_+ + h_-)
\end{aligned}
\tag{2.10}
$$

where $h_+ = z_{j+1} - z_j$ and $h_- = z_j - z_{j-1}$. For $h_+ = h_- = h$ this reduces to (2.9)

2.2.2 Discretization of time derivative:

use eq. (2.4), $A \equiv f$

$$
\frac{p_j^{n+1}}{T_j^{n+1}}\varphi_j^{n+1} - \frac{p_j^n}{T_j^n}\varphi_j^n + \frac{k}{\mu}\left(\rho_{f_j}^{n+1} - \rho_{f_j}^n\right) + \gamma\left.\frac{\partial f}{\partial p}\right|_j^n (p_j^{n+1} - p_j^n) +
$$

$$
+\gamma\left.\frac{\partial f}{\partial T}\right|_j^n (T_j^{n+1} - T_j^n) = \Delta t\left(\partial_z D\varphi \partial_z \frac{p}{T}\right)_j^n
\tag{2.11}
$$

derivatives of the isotherm are not expanded to keep it linear

2.2.3 Complete scheme:

using (2.11) and (2.10)

$$
\begin{aligned}
\xi_j^{n+1} &= \frac{p_j^n}{T_j^n}\varphi_j^n + \frac{k}{\mu}\rho_{f_j}^n + \gamma\left.\frac{\partial f}{\partial p}\right|_j^n p_j^n - \gamma\left.\frac{\partial f}{\partial T}\right|_j^n (T_j^{n+1} - T_j^n) + \\
&\quad \frac{\Delta t}{\Delta z^2}\left[D_j\varphi_j^n\left(\frac{p_{j+1}^n}{T_{j+1}^n} - 2\frac{p_j^n}{T_j^n} + \frac{p_{j-1}^n}{T_{j-1}^n}\right) + \frac{1}{4}(D_{j+1}\varphi_{j+1}^n - D_{j-1}\varphi_{j-1}^n)\left(\frac{p_{j+1}^n}{T_{j+1}^n} - \frac{p_{j-1}^n}{T_{j-1}^n}\right)\right]
\end{aligned}
$$

where $\xi^{n+1} = \dfrac{p^{n+1}}{T^{n+1}} \left(1 - \dfrac{\rho_f^{n+1}}{\rho_{\text{ice}}} \right) + \dfrac{k}{\mu} \rho_f^{n+1} + \gamma \left. \dfrac{\partial f}{\partial p} \right|^n p^{n+1}$

$p \leq p_{sv}(T)$ and $0 \leq \rho_f \leq \rho_{\text{ice}}$
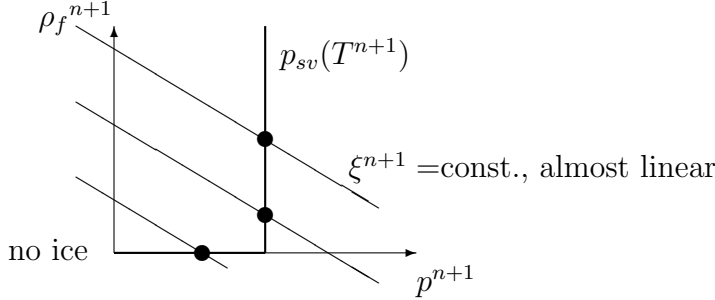
p_{sv} ... saturation vapor pressure

Try $\rho_f^{n+1} = 0 \quad \Rightarrow \quad p^{n+1} = \dfrac{T^{n+1} \cdot \xi^{n+1}}{1 + T^{n+1}\gamma \left. \dfrac{\partial f}{\partial p} \right|^n} \quad$ and $\quad \rho_f^{n+1} = 0$

If $\quad p^{n+1} > p_{sv}(T^{n+1}) \quad$ then $\quad p^{n+1} = p_{sv}(T^{n+1}) \quad$ and

$$\rho_f^{n+1} = \dfrac{\xi^{n+1} - \dfrac{p_{sv}(T^{n+1})}{T^{n+1}} - \gamma \left. \dfrac{\partial f}{\partial p} \right|^n p_{sv}(T^{n+1})}{\dfrac{k}{\mu} - \dfrac{p_{sv}(T^{n+1})}{T^{n+1}\rho_{\text{ice}}}}$$

introduce $\quad p_{\text{frost}}^{n+1} = p_{sv}(T^{n+1})$

2.2.4 Upper boundary condition:

1) $p(z = 0, t) = p_{\text{atm.}}(t)$
2) $D(z = 0) = D_0$
3) $\varphi_0 = 1$

$$\partial_z \left(D\varphi \partial_z \dfrac{p}{T} \right) \Big|_{j=0} = \dfrac{1}{\Delta z^2} \left[D_1\varphi_1 \left(\dfrac{p_2}{T_2} - 2\dfrac{p_1}{T_1} + \dfrac{p_{\text{atm}}}{T_{\text{surf}}} \right) + \dfrac{1}{4}(D_2\varphi_2 - D_0\varphi_0) \left(\dfrac{p_2}{T_2} - \dfrac{p_{\text{atm}}}{T_{\text{surf}}} \right) \right] \quad (2.12)$$

for half-shifted grid $(z_2 = 3z_1)$:

$$a\partial_{zz}b + (\partial_z a)\partial_z b = \dfrac{1}{\Delta z^2} \left[a_1 \left(\dfrac{8}{3}b_s - 4b_1 + \dfrac{4}{3}b_2 \right) + \left(-\dfrac{4}{3}a_s + a_1 + \dfrac{1}{3}a_2 \right) \left(-\dfrac{4}{3}b_s + b_1 + \dfrac{1}{3}b_2 \right) \right]$$
$$(2.13)$$

2.2.5 Lower boundary condition:

no vapor flux (impermeable) $J = 0 \quad \Rightarrow \quad \partial_z \rho_v = 0 \quad \Rightarrow \quad \partial_z \dfrac{p}{T} = 0 \quad \Rightarrow \quad \dfrac{p_{N+1}}{T_{N+1}} = \dfrac{p_{N-1}}{T_{N-1}}$

$$\partial_z \left(D\varphi \partial_z \dfrac{p}{T} \right) \Big|_{j=N} = \dfrac{1}{\Delta z^2} 2D_N\varphi_N \left(\dfrac{p_{N-1}}{T_{N-1}} - \dfrac{p_N}{T_N} \right) \quad (2.14)$$

2.3 Numerical Stability

von Neumann stability analysis has been carried out for various variants of the scheme; this is only relevant for discussion purposes. Typeset notes are available upon request.

Used in Schorghofer and Aharonson (2005)

Bibliography

L. D. Landau and E. M. Lifshitz. *Fluid Mechanics*. Pergamon Press, Oxford, 1987.

N. Schorghofer and O. Aharonson. Stability and exchange of subsurface ice on Mars. *J. Geophys. Res.*, 110(E5):E05003, 2005.

Part 3

Long-Term Ice Evolution

Long-term evolution of sub-surface ice due to loss to space (for asteroids) or exchange with atmosphere (for Mars) using diurnally-resolved temperatures

History:
    2002–2004 equilibrium ice table on Mars
    2006–2011 asynchronous model for ice on Mars (where re-charge can occur)
    2013–2017 asynchronous model for asteroids (where impact-gardening occurs)

3.1   Equilibrium Models of Near-Surface Ice on Mars

The equilibrium depth to the ice table is defined by a balance between the vapor pressure at the ice table and the atmosphere. It is the end result of atmosphere-subsurface vapor exchange after an asymptotically long time. If no equilibrium is possible, then subsurface ice is "unstable". Using the thermal model described in Part 1, this model calculates the equilibrium depth based on matching the vapor density at the ice table and the atmosphere. It is an iterative root-finding procedure, using the bisection method. The iterations are performed by `mars_mapi.f`, which finds the equilibrium depth. Then `mars_mapt2.f` can be used to output a larger number of variables for a given ice table depth.

The model is extensively used in Schorghofer and Aharonson (2005), where further description is available. With extensions described in section 5.1, it also forms the core of the model used in Aharonson and Schorghofer (2006).

3.2   Asynchronous Model for Ice on Mars

Schorghofer (2010) provides a description of this rather complex model, which is not repeated here. In brief, the model couples a diurnally-resolved thermal model with a long-term ice evolution model. Ice can be lost to the atmosphere and vice-versa. Details of the long-term ice evolution model are also described there, which involves a one-sided derivative at the moving ice table, otherwise an instability occurs due to the strong contrast in thermal properties at the ice table. The model allows for up to three layers: dry, soil with interstitial ice (plus air), and massive ice with dust. In the current implementation, one of the two interfaces is tracked explicitly. The model is extensively used in Schorghofer (2007) and Schorghofer and Forget (2012) for studies of the Martian Ice Age cycle.

3.3 Asynchronous Model for Temperature, Impact Stirring, and Ice Loss on Asteroids

Schorghofer (2016) describes this model and applies it to (1) Ceres and (7968) Elst-Pizarro. In brief, it combines diurnally-resolved temperatures, probabilistic impact stirring, and the long-term loss of near-surface ice to space. It was also used for the ice retreat calculations in Prettyman et al. (2017).

A significant complexity in this model arises from partially ice-filled pore spaces (necessary to incorporate the consequences of impact stirring). A simpler two-layer version is made available in `asteroid_fast1`, which is similar to the model described in the supporting information of Sizemore et al. (2017).

Bibliography

O. Aharonson and N. Schorghofer. Subsurface ice on Mars with rough topography. *J. Geophys. Res.*, 111(E11):E11007, 2006.

T. H. Prettyman et al. Extensive water ice within Ceres' aqueously altered regolith. *Science*, 355: 55–59, 2017.

N. Schorghofer. Dynamics of ice ages on Mars. *Nature*, 449(7159):192–194, 2007.

N. Schorghofer. Fast numerical method for growth and retreat of subsurface ice on Mars. *Icarus*, 208(2):598–607, 2010.

N. Schorghofer. Predictions of depth-to-ice on asteroids based on an asynchronous model of temperature, impact stirring, and ice loss. *Icarus*, 276:88–95, 2016.

N. Schorghofer and O. Aharonson. Stability and exchange of subsurface ice on Mars. *J. Geophys. Res.*, 110(E5):E05003, 2005.

N. Schorghofer and F. Forget. History and anatomy of subsurface ice on Mars. *Icarus*, 220(2): 1112–1120, 2012.

H. G. Sizemore et al. Pitted terrain on dwarf planet Ceres and implications for volatiles. *Geophys. Res. Lett*, 2017. in press.

Part 4

Terrestrial Analogs

1-Dimensional Thermal Model with 0-Dimensional Terrestrial Atmosphere

Sun position as a function of date is based on Blanco-Muriel et al. (2001), translated into Fortran. It provides the zenith angle and azimuth of the sun, and the Earth-sun distance. Implemented in `sunpos.f90`

4.1 Mauna Kea atmosphere

calculate clear-sky direct and indirect short-wave irradiance on Mauna Kea in W/m^2
mostly based on Nunez (1980), corrected for typos. Implemented in `mk_atmosphere.f90`

Z ... solar zenith angle (radians)
I_0 ... clear-sky direct irradiance; D_0 ... clear-sky diffuse irradiance
R ... Earth-sun distance in AU
m, m' ... optical air mass (unitless)
p_0 ... total pressure (Pa)
w ... precipitable water vapour (cm)
Transmission coefficients:
ψ_{wa} ... water vapor absorption; ψ_{ws} ... water vapor scattering
ψ_{rs} ... Rayleigh scattering
ψ_{da} ... dust absorption; ψ_{ds} ... dust scattering

Relative air mass:
simplest approximation: $m = 1/\cos Z$
better approximation (Kasten, 1966):

$$m = \frac{1}{\cos Z + 0.15 \times (93.885 - Z)^{-1.253}} \tag{4.1}$$

if $(m < 0)$, then $m = \infty$
$p_0 = 610$ on Mauna Kea summit
$m' = m \times p_0/1013$

Water vapor:
$w = 0.16$ cm for Mauna Kea, according to www.gemini.edu/sciops/telescopes-and-sites/observing-

condition-constraints/mk-water-vapour-statistics

$$\psi_{wa} = 1 - 0.077(wm)^{0.30} \quad \text{McDonald (1960)} \tag{4.2}$$
$$\psi_{ws} = 1 - 0.025wm \tag{4.3}$$

Rayleigh scattering: 8% at sea level according to Fig 3-3 in Bird and Hulstrom (1981)

$$\psi_{rs} = \exp(-0.08m') \tag{4.4}$$

Aerosols: aerosol optical depth on Mauna Kea $= 0.0084 \times (\lambda/1\mu m)^{-1.26}$ (Buton et al., 2013)

$$\psi_{ds} = \exp(-m \times 0.0084 \times 0.5^{-1.26}) \tag{4.5}$$
$$\psi_{da} = \psi_{ds} \quad \text{assumes single scattering albedo of 0.5} \tag{4.6}$$

Direct sunlight:
$$I_0 = \psi_{wa}\psi_{da}\psi_{ws}\psi_{rs}\psi_{ds} \times (\text{solar constant})/R^2 \tag{4.7}$$
(without the last factor, this is the transmittance)

Diffusive sunlight:
$$D_0 = I_0 \cos(Z)\psi_{wa}\psi_{da}\frac{1 - \psi_{ws}\psi_{rs}\psi_{ds}}{2} \tag{4.8}$$

Roundoff issue: if ($D_0 <= 0$), then $D_0 = 0$ because of -0

Total short-wavelength flux:
$$F = I_0 \cos Z + D_0 \tag{4.9}$$

Roundoff issue: if ($F <= 0$), then $F = 0$ because of -0

Not included are the sensible heat flux and long-wave downward radiation.

used in Schorghofer et al. (2017)

4.2 Dry Valleys of Antarctica

This model calculates the loss of buried ice to the atmosphere, and involves molecular diffusion in an air-H_2O mixture, including the advective contribution. The equations underlying this model are described in Schorghofer (2005). The source code has not been readied for distribution and no further documentation was written. This type of model has been superseded by implementations from other research groups. Nevertheless, source code or additional information might be available upon request.

Bibliography

R. E. Bird and R. L. Hulstrom. A simplified clear sky model for direct and diffuse insolation on horizontal surfaces, 1981.

M. Blanco-Muriel, D. C. Alarcón-Padilla, T. López-Moratalla, and M. Lara-Coira. Computing the solar vector. *Solar Energy*, 70:431–441, 2001.

C. Buton et al. Atmospheric extinction properties above Mauna Kea from the Nearby SuperNova Factory spectro-photometric data set. *Astr. & Astrophys.*, 549:A8, 2013.

F. Kasten. *Arch. Meteor. Geophys. Bioklimatol.*, B14:206–223, 1966.

J. E. McDonald. Direct absorption of solar radiation by atmospheric water vapor. *J. Meteor.*, 17: 319–328, 1960.

M. Nunez. The calculation of solar and net radiation in mountainous terrain. *J. Biogeogr.*, 7: 173–186, 1980.

N. Schorghofer. A physical mechanism for long-term survival of ground ice in Beacon Valley, Antarctica. *Geophys. Res. Lett.*, 32:L19503, 2005.

N. Schorghofer, M. Leopold, and K. Yoshikawa. State of high-altitude permafrost on tropical Mauna Kea volcano, Hawaii. *Permafrost and Periglacial Processes*, 2017. in press.

Part 5

Radiative Heat Exchange on Topographic Surfaces

Diffuse Scattering of Short-Wavelength and Infrared on Surface with Topography

History: Planar slopes (sec. 5.1) 2005; 3D topography (sec. 5.2-5.4) 2010–2016

5.1 Thermal Model for Planar Slopes

Thermal Balance for Planar Slopes; coupled 1D Models plus 0D Atmosphere
For Mars, but easily simplified to airless bodies
Planar slopes are much simpler than the general 3D problem

Authors: Implemented by Norbert Schörghofer, with a contribution by Misha Kreslavsky

α ... slope angle

The heat balance on the surface is

$$Q(\alpha) + k \left.\frac{\partial T}{\partial z}\right|_{z=0} = \epsilon\sigma T^4 + \text{(latent heat of CO}_2\text{ frost)} \tag{5.1}$$

with

$$Q = Q_{\text{solar}}(\alpha) + Q_{\text{IR}}(\alpha) + Q_{\text{scat}}(\alpha) + Q_{\text{land}}(\alpha). \tag{5.2}$$

Q is the incoming radiation from the sun, atmosphere, and visible surfaces, T temperature, z the vertical coordinate, k the thermal conductivity, ϵ emissivity, and σ the Stefan-Boltzmann constant.

The elevation β of the sun above an horizontal horizon is given in terms of geographic latitude λ, declination δ of the sun, and the hour angle h:

$$\sin\beta = \cos\lambda\cos\delta\cos h + \sin\lambda\sin\delta. \tag{5.3}$$

The angle θ of the sun above a sloped surface is

$$\sin\theta = \cos\alpha\sin\beta - \sin\alpha\cos\beta\cos(\Delta a), \tag{5.4}$$

where Δa is the difference between the azimuth of the sun and the azimuth of the topographic gradient. The sun is assumed to be below the horizon if either $\sin\beta < 0$ (horizontal horizon at infinity) or $\sin\theta < 0$ (self shadowing of slope).
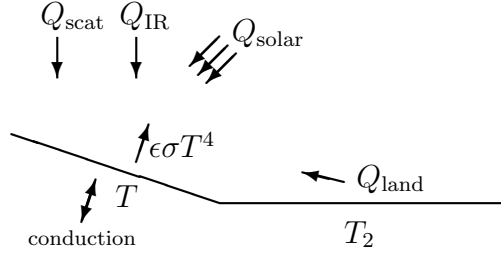
Figure 5.1: Contributions to the heat balance on a slope with surface temperature T.

The direct solar insolation is

$$Q_{\text{solar}} = \frac{S_0}{R^2}(1 - A)(1 - f)^{1/\max(\sin\beta, 0.04)} \sin\theta, \tag{5.5}$$

where S_0 is the solar constant, R the distance from the sun in AU, A the albedo, and f due to the extinction in the atmosphere. The nadir optical depth of the atmosphere is $-\ln(1 - f)$. The length of the path through the atmosphere is proportional to $1/\sin\beta$ and the transmission is taken to be exponential in this path length. The maximum atmospheric path length $\ell_{\max}$ is limited due to the curvature of the planet, $H/\ell_{\max} \approx \sqrt{H/2R} \approx 0.04$ for Mars, where H is the scale height of the atmosphere and R the radius of the planet.

Atmospheric emission is approximated by a fraction f_{IR} (typically 2–4%) of noontime insolation and is kept constant throughout a solar day (Kieffer et al., 1977):

$$Q_{\text{IR}} = f_{\text{IR}} \frac{S_0}{R^2} \cos^2\left(\frac{\alpha}{2}\right) \sin\beta_{\text{noon}} \qquad \text{(all day)} \tag{5.6}$$

The slope factor $\cos^2(\alpha/2)$ for the IR emission takes into account that a tilted surface facing a horizontal horizon sees only a restricted portion of the sky. (This approximation fails in the polar regions; in this case, Kieffer et al. (1977) replaces the noontime insolation with the surface frost emission.)

In addition, there is scattered light when $\sin\beta > 0$, which is approximated by

$$Q_{\text{scat}} = \frac{1}{2} f_{\text{scat}} \frac{S_0}{R^2} \cos^2\left(\frac{\alpha}{2}\right). \tag{5.7}$$

Half of the scattered light is assumed to be lost to space.

The surface reemits radiation in all directions, but receives additional heat from surfaces in its field of view. This emission is weighted according to the incidence angles i and integrated over the spherical angle Ω subtended by the visible land surfaces. If we imagine a horizontal surface at uniform temperature T_2 (Kreslavsky and Head, 2005):

$$Q_{\text{land}} = \epsilon_2 \sigma T_2^4 \int \cos i \, d\Omega = \sin^2\left(\frac{\alpha}{2}\right) \epsilon_2 \sigma T_2^4. \tag{5.8}$$

If one assumes $T_2 = T$ and $\epsilon_2 = \epsilon$, then this term can be brought to the right-hand side of eq. (5.1), leading to an effective emissivity of $\epsilon \cos^2(\alpha/2)$. Otherwise, two 1D models are run simultaneously.

The equation of heat conduction is solved in the subsurface with a semi-implicit Crank-Nicholson scheme on a grid with spatially varying spacings, as described in Part 1 of the User Guide.

Used in Aharonson and Schorghofer (2006); Schorghofer and Edgett (2006)

18

5.2 Horizons and View Factors

Shadowing by nearby topography (terrain shading) defines local horizons and is important for the energy balance. Horizons for each surface element are determined with azimuth rays, typically every 1° in azimuth, and the highest horizon in each direction is stored. For the purpose of horizon calculations, the topography is represented by triangular surface elements. Implemented in `shadows.f90` and `shadow_subs.f90`.

Surface normals are calculated using center-differences in x- and y-direction, and one-sided differences at the domain boundaries. The difference between two angles is evaluated as $\delta = $ mod $(|\alpha_1 - \alpha_2|, 2\pi)$; if $(\delta < 0)$ $\delta \to \delta + 2\pi$; if $(2\pi - \delta < \delta)$ $\delta \to 2\pi - \delta$.

If only shadows are to be calculated, these horizon heights are all that is needed. The shadow calculation method is slower than it could be, but faster than the field of view calculation. The field of view for each surface element is calculated in terms of the spherical angle as viewed from the other element, $d\Omega$, and stored. Mutual visibility is determined by calculating the slope of the line that connects the two elements and comparing it to the maximum topographic slope along a ray in the same direction, tracing outward. (Hence there is a sort involved that is not necessary if only horizons are needed.) For the purpose of view factors, the topography is represented by rectangles. Implemented in `fieldofviews.f90` and `fieldofview_subs.f90`. An optional cut-off radius `RMAX` can be introduced, so spatial distances larger then `RMAX` are ignored. Neighbors in 8 directions are considered.

The topography is defined on a rectangular coordinate grid with spatial resolution Δx in the longitude direction and Δy in the latitude direction. It has no curvature effects, i.e. the domain needs to be small compared to the radius of the body. Nor can the domain include the rotational pole.

5.3 Governing Equations for Scattering

The equation governing the energy balance on the surface is

$$(1 - A)(Q_{\text{direct}} + Q_{\text{refl}}) + k\frac{\partial T}{\partial z} + \epsilon Q_{\text{IR}} = \epsilon \sigma T^4 \tag{5.9}$$

where A is albedo, Q_{direct} incoming solar radiation (insolation), k thermal conductivity, T temperature, z depth below surface, ϵ emissivity, and σ the Stefan-Boltzmann constant. The flux Q_{direct} is determined from the declination of the Sun, latitude, and hour angle, eqs. (5.3, 5.4). Due to topography, reflected sunlight, Q_{refl}, and thermal emission, Q_{IR}, from other surfaces also need to be added.

The amount of sunlight diffusively reflected depends on the spherical angle $d\Omega$ subtended by the surface element, and similarly for infrared emission:

$$Q_{\text{refl}}(x, y) = \frac{1}{\pi} \iint A' \left[Q'_{\text{direct}} + Q'_{\text{refl}} \right] \cos i \, d\Omega(x, y, x', y') \tag{5.10}$$

$$Q_{\text{IR}}(x, y) = \frac{1}{\pi} \iint \left[\epsilon \sigma T'^4 + (1 - \epsilon)Q'_{\text{IR}} \right] \cos i \, d\Omega(x, y, x', y') \tag{5.11}$$

where primed variables are evaluated at (x', y') and unprimed variables at (x, y). The integrals are over all surface elements within the field of view, and i is the local incidence angle. Equations (5.10) and (5.11) turn into an explicit time-stepping procedure when Q'_{refl} and Q'_{IR} on the right hand side are evaluated at the previous time step. The term with the factor $(1 - \epsilon)$ is reflected infrared.

The model also includes 1D subsurface heat conduction (1.1), and is treated as described in Part 1. Subsurface temperatures need to be equilibrated, and hence the entire model needs to be run much longer than with equilibrium surface temperatures. Lateral subsurface heat conduction is neglected. Without subsurface conduction, equilibrium temperatures, according to eq. (5.9) with $k = 0$, are used, and only a few steps of equilibration are needed.

5.4   Algorithm

The algorithm is separated into two parts.

The first determines the field of view, horizons, and subtended angles (view factors) of all surface elements with all other surface elements. This information is written to files `horizons.dat` and `fieldofviews.dat`. This part is easily parallelized, as calculations for each pixel are independent of one another although the entire topography has to be loaded into memory. For parallelization, one column or row of the spatial domain is run on one CPU core. The horizons file is rectangular, with the number of entries equals (number of azimuths)×(number of topographic pixels). The fieldofviews file is giant and it is not rectangular. Each line in the output file corresponds to a topographic pixel and at the beginning specifies the number of pixels in the field of view. Each visible pixel has then three numbers stored with it: The x and y indices of the pixel and the view factor. Non-visible pixels are not stored. When these data are read in later, they are stored as 2-byte integers and 4-byte floating point numbers respectively, half of what is common, to save memory.

The second part simulates the time evolution of illumination and surface temperature, using the horizons and (optionally) the field of view as input. The surface energy balance is integrated over time at steps of a fraction (e.g., 1/100th) of a solar day. Surface temperature and illumination are updated at every time step, and thus reflection is taken into account to the order of the number of time steps within a solar day, which is large. The time step is explicit, but the subsurface model, if used, is semi-implicit.

Bibliography

O. Aharonson and N. Schorghofer. Subsurface ice on Mars with rough topography. *J. Geophys. Res.*, 111(E11):E11007, 2006.

H. H. Kieffer, T. Z. Martin, A. R. Peterfreund, B. M. Jakosky, E. D. Miner, and F. D. Palluconi. Thermal and albedo mapping of Mars during the Viking primary mission. *J. Geophys. Res.*, 82: 4249, 1977.

M. A. Kreslavsky and J. W. Head. Mars at very low obliquity: atmospheric collapse and the fate of volatiles. *Geophys. Res. Lett.*, 32(12):L12202, 2005.

N. Schorghofer and K. S. Edgett. Seasonal surface frost at low latitudes on Mars. *Icarus*, 180(2): 321–334, 2006.

Part 6

Surface-bounded Exospheres

Monte Carlo Model of Ballistically Hopping Molecules

History: developed 2012–2017
Core routines are implemented in `montecarlo.f90`

6.1 Introduction

The ballistic trajectories of the molecules in a surface-bounded exosphere is simulated with a Monte-Carlo method. Individual water molecules are launched with a probabilistically distributed cartesian velocity components that amount to a random initial azimuth and thermal speed appropriate for the local surface temperature. The model then computes the molecule's impact location and time analytically. An event-driven algorithm is used, where landing and launching events are processed in time-order. Events are scheduled and processed until the molecule is destroyed or lost or until its landing or launch time is beyond the next thermal model time step, when surface temperatures are updated.

Each molecule has a longitude $p_r[1]$, latitude $p_r[2]$, status p_s (on surface =0, in-flight =1, lost or cold-trapped < 0), and time to the next event p_t (until it arrives on surface or until it will leave the surface). Negative status values can be used to distinguish where it is trapped or how it was lost. Surface temperatures are calculated with a 1D thermal model, as in Part 1.

6.2 Ballistic Flight on Sphere

d ... flight distance
t ... time of flight
τ_{res} ... surface residence time
τ_{dissoc} ... photo-destruction time
v_{esc} ... escape speed
v_1 ... velocity along longitude direction
v_2 ... velocity along meridian
v_3 ... vertical velocity component
az ... azimuth
$\Delta\phi$ ... difference in longitude
λ ... latitude
M ... molar mass

R_{moon} ... radius of body

The ballistic molecule moves on a plane that goes through the center of sphere/body; the ground track is thus part of a great circle.

Each of the three velocity components is picked from a Gaussian distribution, which involves a scaling factor of $\sqrt{T_{\text{surf}} 8314.5/M}$. This will lead to a Maxwellian velocity distribution and uniformly distributed launch azimuths. Other probability distributions can be implemented, if desired.

For constant g,

$$t = 2v_3/g \tag{6.1}$$

$$d = \frac{2}{g}v_3\sqrt{v_1^2 + v_2^2} \tag{6.2}$$

If $|v| > 0.4v_{\text{esc}}$, then use non-uniform gravity formula
If $|v| > v_{\text{esc}}$, then gravitational escape

$$az = \texttt{atan2}(v_2, v_1) \tag{6.3}$$

$$\cos(az) = v_2/\sqrt{v_1^2 + v_2^2} \tag{6.4}$$

$$\sin\varphi_2 = \sin(d/R_{\text{moon}})\cos(\lambda)\cos(az) + \sin(\lambda)\cos(d/R_{\text{moon}}) \tag{6.5}$$

$$p_r(2) = \arcsin(\sin\varphi_2) \tag{6.6}$$

$$\cos\varphi_2 = \sqrt{1 - \sin^2\varphi_2} \tag{6.7}$$

$$\cos(\Delta\phi) = \frac{\cos(d/R_{\text{moon}})\cos(\lambda) - \sin(\lambda)\sin(d/R_{\text{moon}})\cos(az)}{\cos\varphi_2} \tag{6.8}$$

Roundoff issues: if $\cos(\Delta\phi) > +1$ then $\cos(\Delta\phi) = +1$; if $\cos(\Delta\phi) < -1$ then $\cos(\Delta\phi) = -1$.

$\Delta\phi = \arccos(\cos(\Delta\phi))$
if $v_1 < 0$, then $\Delta\phi = -\Delta\phi$
$p_r(1) = p_r(1) + \Delta\phi$
if $(\cos\varphi_2 == 0)$ then on pole
$p_r(1)$ is normalized to 0...360°.

$p_t = p_t + t$

6.3   Other Model Components

6.3.1   Photo-destruction

Molecules are lost in-flight by photo-destruction (Table 6.1), at a rate of $t/(\tau_{\text{dissoc}}R^2)$, where R is the distance from the sun, often approximated by the semi-major axis. Require incident flux $Q > 0$, since this only occurs on the dayside. A comprehensive compilation of photo-destruction rates can be found in Huebner et al. (1992).

6.3.2   Coriolis effect

The Coriolis effect is incorporated by adding tangential velocities but subtracting the distance the surface has traveled during time of flight.

	M	τ_{dissoc}	
H_2O	18.015	20×3600	Potter and del Duca (1964)
H_2O		1/12.6e-6	Crovisier (1989), normal sun
H_2O		1/23.0e-6	Crovisier (1989), active sun
HDO	19.021		
He-4	4.0026	1.9e7	Killen and Ip (1999)
Ar-40	39.962	3.2e6	Killen and Ip (1999)

Table 6.1: Some pertinent parameters. τ_{dissoc} = photodissociation time scale at 1 AU

At launch:

$$v_1 = v_1 - \frac{2\pi R_{\mathrm{moon}}}{\mathrm{siderealDay}} \cos(p_r(2)) \tag{6.9}$$

After landing:

$$p_r(1) = p_r(1) + t/\mathrm{siderealDay} \tag{6.10}$$

The Coriolis effect is negligible on the Moon and on Mercury, but noticeable on Ceres.

6.3.3 Event driver

Process events over the time step of the thermal model Δt_T, e.g., one hour

```
if (p_t > Δt_T) exit
case(p_s < 0) exit !  not alive
case(p_s==0) !  leaving
    hop once, update p_t
case(p_s==1) !  landing
    if (incoldtrap) then
       p_t = ∞
       cycle
    endif
    evaluate τ_res(T_surf)
    p_t = p_t + τ_res
```

After all events within Δt_T are processed, subtract Δt_T from all times: if $(\mathtt{p_s} >= 0)$ $p_t = p_t - \Delta t_T$. (Moving time zero helps avoid truncation errors after a long run.)

6.3.4 Residence times

E ... sublimation rate/flux
θ ... number of H_2O molecules per area
$\theta_m = 1e19 m^{-2}$ ... areal density of H_2O monolayer
T ... local surface temperature

Temperature also sets the residence time of water molecules on the surface, which is negligible on most of the dayside and very long on most of the nightside. Many models use a binary choice, where molecules either immediately hop on the day side or reside indefinitely on the surface on the

night side. This model uses a molecular residence time that depends continuously on temperature instead of a threshold.

For crystalline ice, the average molecular surface residence time only depends on T, but for adsorbed water it is also a function of the adsorbate density θ. The model uses the parametrization $\tau_{\text{res}} = c\theta_m/E(T)$, where E is the sublimation rate of pure ice. For pure ice $c = 1$. For example, $c = 1/400$ is reasonable for 0.1 monolayers (Schorghofer and Aharonson, 2014). The functional form is almost the same as using a vibration frequency multiplied by a Boltzmann factor.

For non-condensible species, e.g. He, $\tau_{\text{res}} = 0$.

6.4 Non-uniform Gravity

ballistic travel distance and flighttime with radial dependence of gravitational acceleration; not suitable for small velocities due to roundoff. This effect is negligible for Mercury and small on the Moon, but necessary for Ceres. Equations are derived from those in Vogel (1966) and Kegerreis (2015).

e ... eccentricity of ballistic trajectory
α ... zenith angle of launch velocity, $\alpha = \arctan\left(\sqrt{v_1^2 + v_2^2}/v_3\right)$

$$\gamma = (|v|/v_{\text{esc}})^2 \tag{6.11}$$

$$a = \frac{R_{\text{moon}}}{2(1-\gamma)} \tag{6.12}$$

$$e = \sqrt{1 - 4\gamma(1-\gamma)\sin^2\alpha} \tag{6.13}$$

$$d = 2R_{\text{moon}}\arccos\left(\frac{1}{e}(1 - 2\gamma\sin^2\alpha)\right) \tag{6.14}$$

$$E_p = \pi - 2\arctan\left(\sqrt{\frac{1-e}{1+e}}\middle/ \tan\frac{d}{4R_{\text{moon}}}\right) \tag{6.15}$$

$$t = 2\sqrt{\frac{2a^3}{R_{\text{moon}}v_{\text{esc}}^2}}(E_p + e\sin E_p) \tag{6.16}$$

Round-off issues:
a) If e is very close to 1, then based on Taylor expansion of (6.14) and (6.15)

$$d = 4\gamma R_{\text{moon}}\sin\alpha \tag{6.17}$$

$$E_p = \pi - 2\arctan\sqrt{\frac{1-\gamma}{\gamma}} \tag{6.18}$$

b) If $1 - 2\gamma\sin^2\alpha > e$ (horizontal launch), do something, otherwise $d = \texttt{NaN}$

Used in Schorghofer (2014) (uniform gravity) and Schorghofer et al. (2016, 2017) (non-uniform gravity).

Bibliography

J. Crovisier. The photodissociation of water in cometary atmospheres. *Astr. Astrophys.*, 213: 459–464, 1989.

W. F. Huebner, J. J. Keady, and S. P. Lyon. Solar photo rates for planetary atmospheres and atmospheric pollutants. *Astrophys. Space Sci.*, 195:1–294, 1992.

J. Kegerreis. Bouncing on the moon. Master's thesis, Durham University, 2015.

R. M. Killen and W.-H. Ip. The surface-bounded atmospheres of Mercury and the Moon. *Rev. Geophys.*, 37(3):361–406, 1999.

A. E. Potter and B. del Duca. Lifetime in space of possible parent molecules of cometary radicals. *Icarus*, 3:103, 1964.

N. Schorghofer. Migration calculations for water in the exosphere of the Moon: Dusk-dawn asymmetry, heterogeneous trapping, and D/H fractionation. *Geophys. Res. Lett.*, 41:4888–4893, 2014.

N. Schorghofer and O. Aharonson. The lunar thermal ice pump. *Astrophys. J.*, 788:169, 2014.

N. Schorghofer, E. Mazarico, T. Platz, F. Preusker, S.E. Schröder, C.A. Raymond, and C.T. Russell. The permanently shadowed regions of dwarf planet Ceres. *Geophys. Res. Lett.*, 43:6783–6789, 2016.

N. Schorghofer, P. Lucey, and J.-P. Williams. Theoretical time variability of mobile water on the moon and its geographic pattern. *Icarus*, 2017. in press.

U. Vogel. Molecular fluxes in the lunar atmosphere. *Planet. Space Sci.*, 14:1233–1252, 1966.